Genetic and cellular evidence of vascular inflammation in neurofibromin-deficient mice and humans

Elisabeth A. Lasater,[1,2] Fang Li,[1,3] Waylan K. Bessler,[1,3] Myka L. Estes,[1,3] Sasidhar Vemula,[1,3] Cynthia M. Hingtgen,[4] Mary C. Dinauer,[1,3] Reuben Kapur,[1,2,3] Simon J. Conway,[1,2,3] and David A. Ingram Jr.[1,2,3]

[1]Herman B. Wells Center for Pediatric Research, [2]Department of Biochemistry and Molecular Biology, [3]Department of Pediatrics, and [4]Department of Neurology, Indiana University School of Medicine, Indianapolis.

Neurofibromatosis type 1 (NF1) results from mutations in the *NF1* tumor suppressor gene, which encodes the protein neurofibromin. NF1 patients display diverse clinical manifestations, including vascular disease, which results from neointima formation and vessel occlusion. However, the pathogenesis of NF1 vascular disease remains unclear. Vessel wall homeostasis is maintained by complex interactions between vascular and bone marrow–derived cells (BMDCs), and neurofibromin regulates the function of each cell type. Therefore, utilizing *cre/lox* techniques and hematopoietic stem cell transplantation to delete 1 allele of *Nf1* in endothelial cells, vascular smooth muscle cells, and BMDCs alone, we determined which cell lineage is critical for neointima formation in vivo in mice. Here we demonstrate that heterozygous inactivation of *Nf1* in BMDCs alone was necessary and sufficient for neointima formation after vascular injury and provide evidence of vascular inflammation in $Nf1^{+/-}$ mice. Further, analysis of peripheral blood from NF1 patients without overt vascular disease revealed increased concentrations of inflammatory cells and cytokines previously linked to vascular inflammation and vasoocclusive disease. These data provide genetic and cellular evidence of vascular inflammation in NF1 patients and $Nf1^{+/-}$ mice and provide a framework for understanding the pathogenesis of NF1 vasculopathy and potential therapeutic and diagnostic interventions.

Introduction

Neurofibromatosis type 1 (NF1) is an autosomal dominant disorder that results from mutations in the tumor suppressor gene *NF1* (1). Neurofibromin, the protein product of *NF1*, functions as a $p21^{Ras}$ (Ras) GTPase-activating protein (GAP) to negatively regulate Ras activity (2). More than 240 different mutations have been described within the *NF1* gene, all of which result in little or no protein product (3). While loss of heterozygosity has been described in primary tumor samples (4), the germline mutations that cause NF1 affect only 1 copy of the *NF1* gene. Haploinsufficiency of *NF1* results in disease with complete penetrance and a range of clinical complications.

The most common clinical manifestations of NF1 include dermal and plexiform neurofibromas, learning deficits, and skeletal abnormalities. Vascular disease associated with NF1 is an underrecognized complication that results in increased morbidity and mortality, particularly among younger patients (5, 6). In 2001, an analysis of 3,253 death certificates of persons with NF1 indicated that the median age of death for NF1 patients was 15 years lower that of the general population (6). In this report, a diagnosis suggestive of NF1 vasculopathy was listed 7.2 times more often than expected among NF1 patients less than 30 years old at time of death and 2.2 times more often than expected among patients 30–40 years old at the time of death (6). Another study demonstrated that 2.5% of children with NF1 who had undergone brain MRI were found to have cerebrovascular system abnormalities including narrowed vessels, moyamoya, vascular stenosis, and aneurysm (7). NF1 patients are not routinely screened for vascular disease, and therefore the natural history, frequency and pathogenesis of vascular lesion formation are not well defined despite numerous clinical observations of NF1 vasculopathy. NF1 vasoocclusive lesions are characterized by an accumulation of VSMCs within the intima area of the vessel, termed neointima formation (8). Despite recent advances utilizing in vivo models, the mechanism of NF1 vascular lesion formation is not understood.

A model of NF1 vasculopathy has previously been described in which *Nf1* was completely ablated in VSMCs (9). However, in this model, a phenotype that recapitulates human vasoocclusive disease was only evident on a haploinsufficient background, suggesting the role of another cell lineage in NF1 vascular disease (9). Similarly, we recently developed a murine model of NF1 vasculopathy in $Nf1^{+/-}$ mice that is reminiscent of the vascular lesions described in patients (10). We demonstrated that $Nf1^{+/-}$ mice have increased neointima formation in response to arterial injury compared with WT controls that was characterized by increased VSMC proliferation and accumulation of inflammatory cells (10). Infiltration of inflammatory cells into the vessel wall is characteristic of vascular inflammation. Therefore, excessive infiltration of $Nf1^{+/-}$ inflammatory cells into the neointima is an important observation, since chronic inflammation may promote EC senescence and increased VSMC proliferation (11, 12) in NF1 patients, resulting in vascular lesion formation. Neurofibromin has clearly been established as a critical regulator of EC, VSMC, and BM cell function in vitro and in vivo in response to multiple growth factors implicated in vessel wall homeostasis and neointima formation (13–16). However, despite these observations, it remains unclear which cell lineage(s) are the major contributor to neointima formation in $Nf1^{+/-}$ mice, and this determination is essen-

Conflict of interest: The authors have declared that no conflict of interest exists.
Citation for this article: *J Clin Invest.* 2010;120(3):859–870. doi:10.1172/JCI41443.

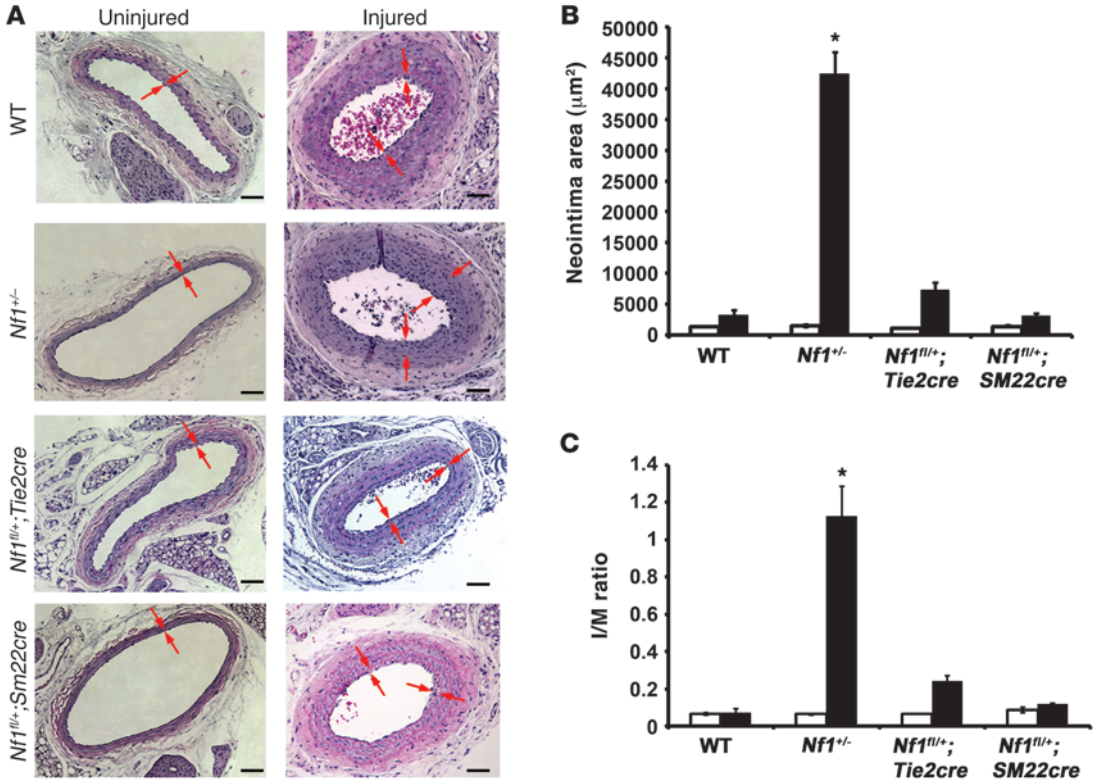

Figure 1
Histological and morphometric analysis of WT, *Nf1*$^{+/-}$, *Nf1*$^{fl/+}$*;Tie2cre*, and *Nf1*$^{fl/+}$*;SM22cre* mice. (**A**) Representative H&E-stained cross sections of uninjured and injured carotid arteries from WT, *Nf1*$^{+/-}$, *Nf1*$^{fl/+}$*;Tie2cre*, and *Nf1*$^{fl/+}$*;SM22cre* mice. Red arrows indicate neointima boundaries. Scale bars: 50 μm. (**B** and **C**) Quantification of neointima area (**B**) and I/M ratio (**C**) of uninjured (white bars) and injured (black bars) carotid arteries from WT, *Nf1*$^{+/-}$, *Nf1*$^{fl/+}$*;Tie2cre*, and *Nf1*$^{fl/+}$*;SM22cre* mice. Data represent the mean of 3 arterial cross sections (400, 800, and 1,200 μm proximal to the ligation) ± SEM, $n = 4–7$. *$P < 0.001$ for *Nf1*$^{+/-}$ uninjured versus *Nf1*$^{+/-}$ injured and for *Nf1*$^{+/-}$ injured versus WT injured, *Nf1*$^{fl/+}$*;Tie2cre* injured, and *Nf1*$^{fl/+}$*;SM22cre* injured, by 1-way ANOVA with Tukey's post-hoc test.

tial to understand the pathophysiology of NF1 vascular disease and potential therapeutic interventions.

Utilizing *cre/lox* technology and adoptive hematopoietic stem cell transfer techniques, we generated mice that were heterozygous for *Nf1* in VSMCs, ECs, or bone marrow–derived cells (BMDCs) to dissect the role of each cell lineage independently in neointima formation. Surprisingly, heterozygous inactivation of *Nf1* in VSMCs or ECs alone or in combination was insufficient to recapitulate neointima formation of *Nf1*$^{+/-}$ mice. However, BM transfer experiments directly implicated *Nf1*$^{+/-}$ BMDCs as necessary and sufficient for vasoocclusive disease in mice. Parallel studies in peripheral blood samples of NF1 patients revealed cellular and cytokine evidence of chronic inflammation. Therefore, these studies provide the first evidence to our knowledge that chronic inflammation is an important contributor to NF1 vasculopathy and provide the platform for future design of biomarkers and interventional trials.

Results

Heterozygous inactivation of *Nf1* in endothelial cells and VSMCs alone is insufficient to recapitulate neointima formation of *Nf1*$^{+/-}$ mice. We previously demonstrated that *Nf1*$^{+/-}$ mice have increased neointima formation compared with WT controls, reminiscent of NF1 vasculopathy (10). In order to determine the cellular mechanism of NF1 vasculopathy, we initially generated mice, utilizing *cre/lox* technology, that were heterozygous for *Nf1* in ECs alone or VSMCs alone. Briefly, *Nf1*$^{fl/fl}$ mice, which contain conditional *Nf1* alleles susceptible to Cre-mediated recombination, were crossed with either *Tie2cre* (17) or *SM22cre* (18) mice to generate *Nf1*$^{fl/+}$*;Tie2cre* or *Nf1*$^{fl/+}$*;SM22cre* progeny. As previously demonstrated, *Nf1*$^{fl/fl}$ mice effectively undergo Cre-mediated recombination when crossed with either the *Tie2cre* (19) or *SM22cre* (9) transgenic mice, generating mice with heterozygous inactivation of *Nf1* specifically in ECs or VSMCs, respectively. Of note, Tie2cre expression is not limited solely to the ECs but can also be detected in BM cells (20, 21). Quantitative PCR demonstrated that approximately 25% of BMDC in our *Nf1*$^{fl/+}$*;Tie2cre* mice expressed Cre, and some Nf1 recombination was observed in the BM from these animals (data not shown).

To interrogate the role of *Nf1* in ECs and VSMCs, *Nf1*$^{fl/+}$*;Tie2cre* and *Nf1*$^{fl/+}$*;SM22cre* mice, respectively, underwent carotid artery ligation and analysis for neointima formation along with *Nf1*$^{fl/-}$ (*Nf1*$^{+/-}$) and *Nf1*$^{fl/+}$ (WT) experimental controls. Carotid artery ligation is a well-established model that induces neointima formation through changes in hemodynamic forces (22). Briefly, the common carotid artery was completely ligated proximal to the bifurcation, and the mice recovered for 28 days postoperatively. Whole ligated carotid arteries along with the contralateral uninjured carotid arteries were harvested from each animal and analyzed for neointima formation as previously described (22). The neointima

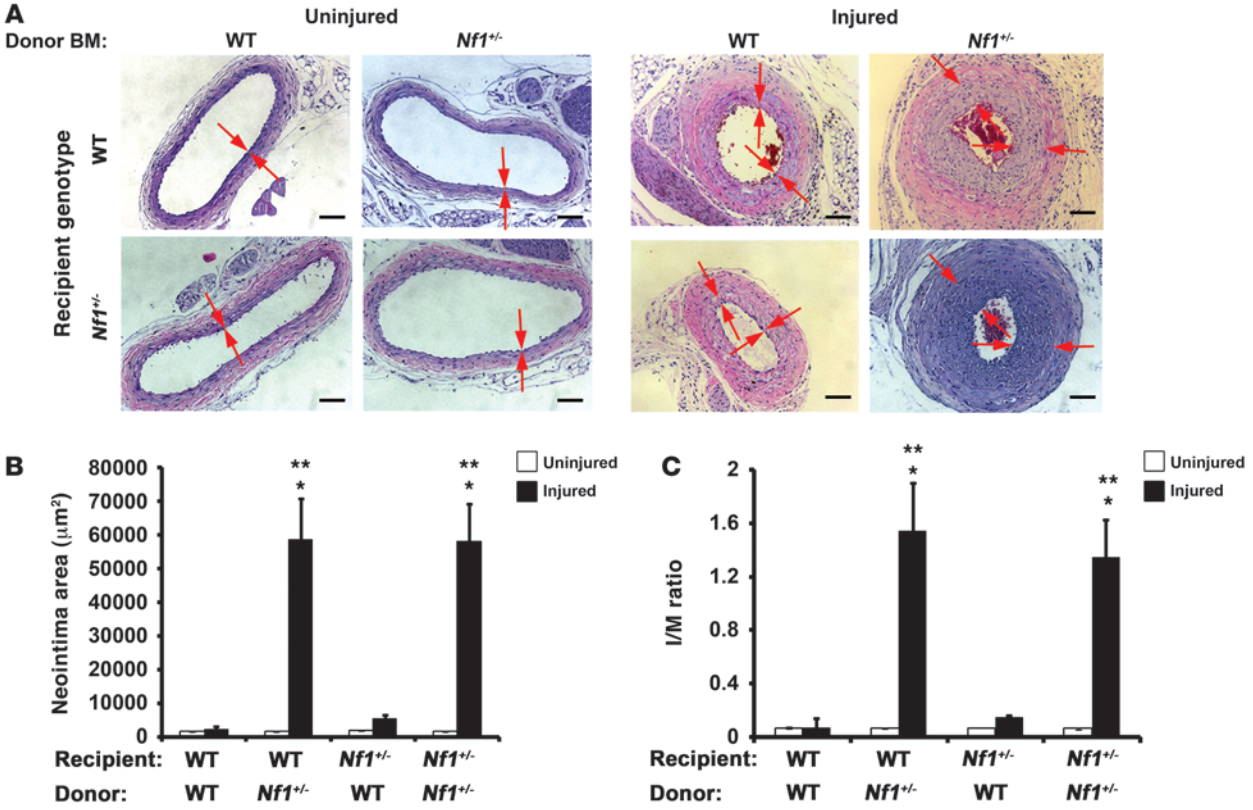

Figure 2

Histological and morphometric analysis of WT and *Nf1*$^{+/-}$ mice transplanted with WT and *Nf1*$^{+/-}$ BM. (**A**) Representative H&E-stained cross sections of uninjured and injured carotid arteries from WT and *Nf1*$^{+/-}$ mice transplanted with WT or *Nf1*$^{+/-}$ BM. Red arrows indicate boundaries of neointima. Scale bars: 50 μm. (**B** and **C**) Quantification of neointima area (**B**) and I/M ratio (**C**) of uninjured and injured carotid arteries from WT or *Nf1*$^{+/-}$ recipients transplanted with WT or *Nf1*$^{+/-}$ BM. Data represent the mean neointima area of 3 arterial cross sections (400, 800, and 1200 μm distal to the ligation) ± SEM, $n = 5–8$. *$P < 0.001$ for WT mice transplanted with *Nf1*$^{+/-}$ BM uninjured versus WT mice transplanted with *Nf1*$^{+/-}$ BM injured and for *Nf1*$^{+/-}$ mice transplanted with *Nf1*$^{+/-}$ BM uninjured versus *Nf1*$^{+/-}$ mice transplanted with *Nf1*$^{+/-}$ BM injured; **$P < 0.001$ for WT mice transplanted with *Nf1*$^{+/-}$ BM and *Nf1*$^{+/-}$ mice transplanted with *Nf1*$^{+/-}$ BM versus WT mice transplanted with WT BM and *Nf1*$^{+/-}$ mice transplanted with WT BM injured, by 1-way ANOVA with Tukey's post-hoc test.

area is defined as the cellular area between the lumen of the vessel and the internal elastic lamina.

Histological analysis of H&E-stained sections from the uninjured carotid artery demonstrated that WT, *Nf1*$^{+/-}$, *Nf1*$^{fl/+}$*;Tie2cre*, and *Nf1*$^{fl/+}$*;SM22cre* were not structurally different and showed no sign of neointima formation (Figure 1A). Analysis of the ligated carotid arteries indicated that only *Nf1*$^{+/-}$ mice had significantly enhanced neointima formation in response to arterial injury (Figure 1, B and C, and Supplemental Figure 1; supplemental material available online with this article; doi:10.1172/JCI41443DS1), with no difference in neointima formation detected between WT, *Nf1*$^{fl/+}$*;Tie2cre*, and *Nf1*$^{fl/+}$*;SM22cre* mice. Specifically, *Nf1*$^{+/-}$ mice had a 5-fold increase in intima/media (I/M) ratio compared with WT, *Nf1*$^{fl/+}$*;Tie2cre*, and *Nf1*$^{fl/+}$*;SM22cre* mice (Figure 1C). These data demonstrate that heterozygous inactivation of *Nf1* in ECs or VSMCs alone is insufficient for neointima formation in *Nf1*$^{+/-}$ mice after vascular injury. Minimal neointima formation after carotid injury in WT C57BL/6 or mixed C57BL/6 × 129SvJ mice is consistent with previous reports (23).

Nf1$^{+/-}$ *BMDCs are necessary and sufficient for neointima formation.* Previous reports have demonstrated that infiltration of BMDCs, especially leukocytes and macrophages, significantly contributes to neointima formation (24). We previously reported that *Nf1*$^{+/-}$ BMDCs, especially myeloid cells, have increased migration and proliferation in response to multiple growth factors implicated in neointima formation (13, 14). Therefore, to test the hypothesis that *Nf1*$^{+/-}$ BMDCs enhanced neointima formation, we utilized adoptive hematopoietic stem cell transfer techniques. Specifically, BMDCs isolated from *Nf1*$^{+/-}$ or WT mice that ubiquitously express GFP were transplanted into conditioned *Nf1*$^{+/-}$ or WT recipients to generate *Nf1*$^{+/-}$ mice reconstituted with either WT or *Nf1*$^{+/-}$ GFP BM and WT mice reconstituted with either WT or *Nf1*$^{+/-}$ GFP BM. BM engraftment was determined after 4 months by determining the percentage of GFP-positive mononuclear cells (MNCs) in peripheral blood by flow cytometric analysis. Mice with greater than 85% engraftment (Supplemental Figure 2) underwent carotid artery ligation as previously described (22).

Uninjured arteries from each transplant group were morphologically similar and showed no evidence of neointima formation (Figure 2). In response to carotid artery ligation, *Nf1*$^{+/-}$ mice transplanted with WT BM had a 10-fold reduction in neointima area (Figure 2, A and B, and Supplemental Figure 3) and a 9-fold

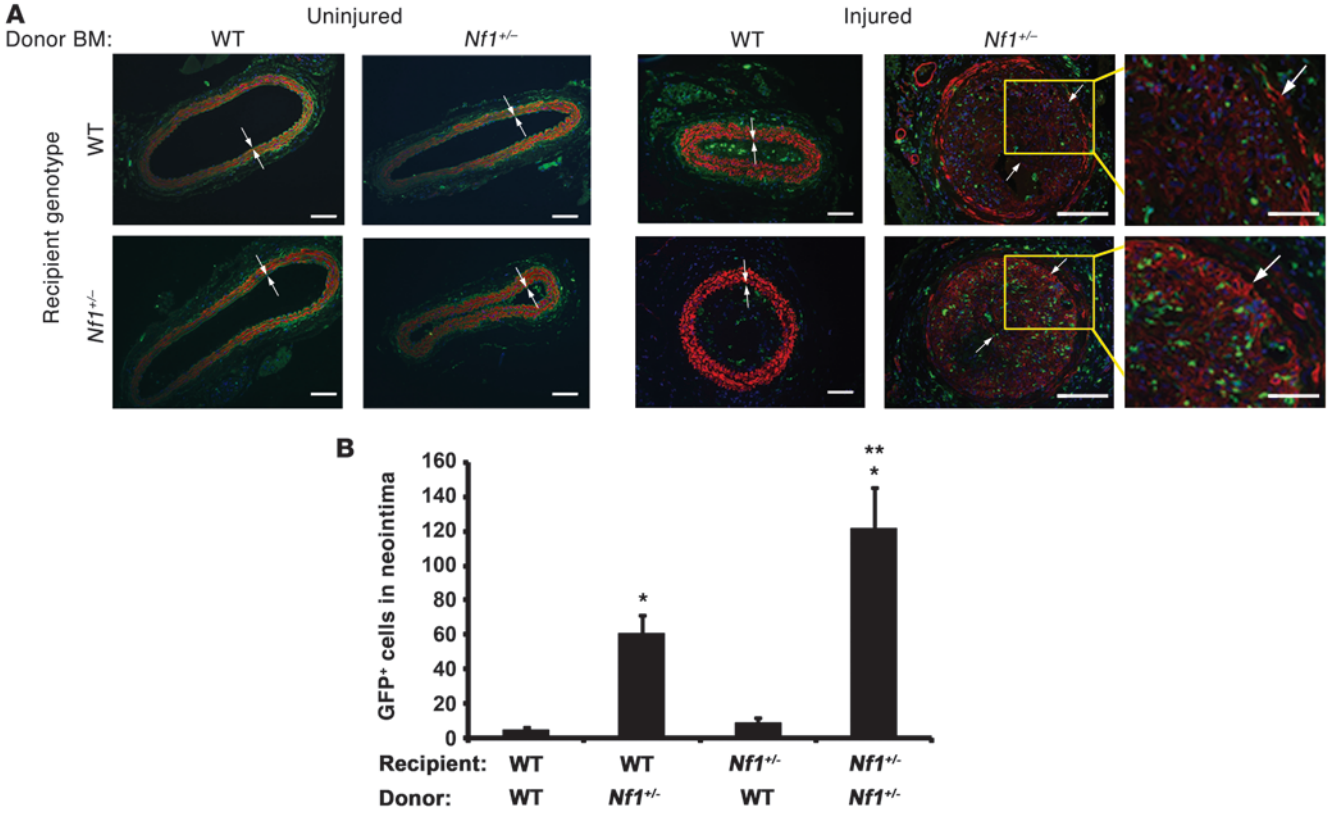

Figure 3

Identification of VSMCs and BMDCs within the neointima of WT and *Nf1*$^{+/-}$ mice transplanted with WT and *Nf1*$^{+/-}$ BM. (**A**) Representative photomicrographs of uninjured and injured carotid arteries from WT and *Nf1*$^{+/-}$ mice transplanted with either WT or *Nf1*$^{+/-}$ BM stained with anti–α-SMA (red) antibody to identify VSMCs and anti-GFP (green) antibody to identify BMDCs. Cell nuclei are visible by DAPI stain (blue), and some tissue autofluorescence is visible (green). White arrows indicate neointima boundaries. Yellow boxes identify area of injured WT and *Nf1*$^{+/-}$ mice transplanted with *Nf1*$^{+/-}$ BM magnified in the far-right panels. Scale bars: 50 μm; far-right panels, 250 μm. (**B**) Quantification of the total number of GFP-positive cells within the neointima of WT and *Nf1*$^{+/-}$ recipient mice after carotid ligation. Data represent the mean GFP-positive cells within the neointima 600 μm proximal to the ligation ± SEM, $n = 6$. *$P < 0.05$ for injured WT mice transplanted with *Nf1*$^{+/-}$ BM versus injured WT mice transplanted with WT BM and for injured *Nf1*$^{+/-}$ mice transplanted with *Nf1*$^{+/-}$ BM versus injured *Nf1*$^{+/-}$ mice transplanted with WT BM; **$P < 0.05$ for injured *Nf1*$^{+/-}$ mice transplanted with *Nf1*$^{+/-}$ BM versus injured WT mice transplanted with *Nf1*$^{+/-}$ BM, by 1-way ANOVA with Tukey's post-hoc test.

reduction in I/M ratio compared with *Nf1*$^{+/-}$ mice reconstituted with *Nf1*$^{+/-}$ BM (Figure 2C). Further, WT mice transplanted with *Nf1*$^{+/-}$ BM had a 20-fold increase in neointima area (Figure 2B) and I/M ratio (Figure 2B) compared with WT mice reconstituted with WT BM. The observation that transplantation of WT BM into *Nf1*$^{+/-}$ mice completely abrogated neointima formation indicates that heterozygous inactivation of *Nf1* in BMDCs is necessary and sufficient for neointima formation in response to vascular injury.

Nf1$^{+/-}$ *mice have evidence of vascular inflammation*. To further understand the cellular mechanism of *Nf1*$^{+/-}$ BMDCs in neointima formation, we identified BMDCs within the neointima in response to injury. Utilizing immunohistochemistry, we costained uninjured and injured carotid artery cross sections from each transplant group with an anti-GFP antibody, to identify BMDCs, and an anti–α-SMA antibody, to identify VSMCs. We utilized an anti-GFP antibody given the amount of autofluorescence inherent in murine tissue. Uninjured carotid arteries for each transplant group showed no accumulation of BMDCs within the vessel (Figure 3A). In response to injury, WT mice transplanted with *Nf1*$^{+/-}$ BM had a 12-fold increase in the accumulation of GFP-positive BMDCs within the neointima compared with WT mice reconstituted with WT BM (Figure 3). Similarly, *Nf1*$^{+/-}$ mice transplanted with *Nf1*$^{+/-}$ BM had a 14-fold increase in the number of GFP-positive BMDCs within the neointima compared with *Nf1*$^{+/-}$ mice transplanted with WT BM (Figure 3B). Surprisingly, despite no difference in neointima size, *Nf1*$^{+/-}$ mice transplanted with *Nf1*$^{+/-}$ BM had a 2-fold increase in the number of GFP-positive BMDCs within the neointima compared with WT mice transplanted with *Nf1*$^{+/-}$ BM in response to carotid ligation (Figure 3B), with no difference in the total number of cells within the neointima. This observation indicates that heterozygous inactivation of *Nf1* in other cell lineages enhances the recruitment/survival of BMDCs in *Nf1*$^{+/-}$ mice transplanted with *Nf1*$^{+/-}$ BM. Of note, arterial cross sections showed no colocalization of GFP-positive cells with α-SMA–positive cells (Figure 3A), indicating that the VSMCs within the neointima are locally derived and not BM-derived VSMCs.

To further define the cellular mechanism of enhanced neointima formation in *Nf1*$^{+/-}$ mice transplanted with *Nf1*$^{+/-}$ BM,

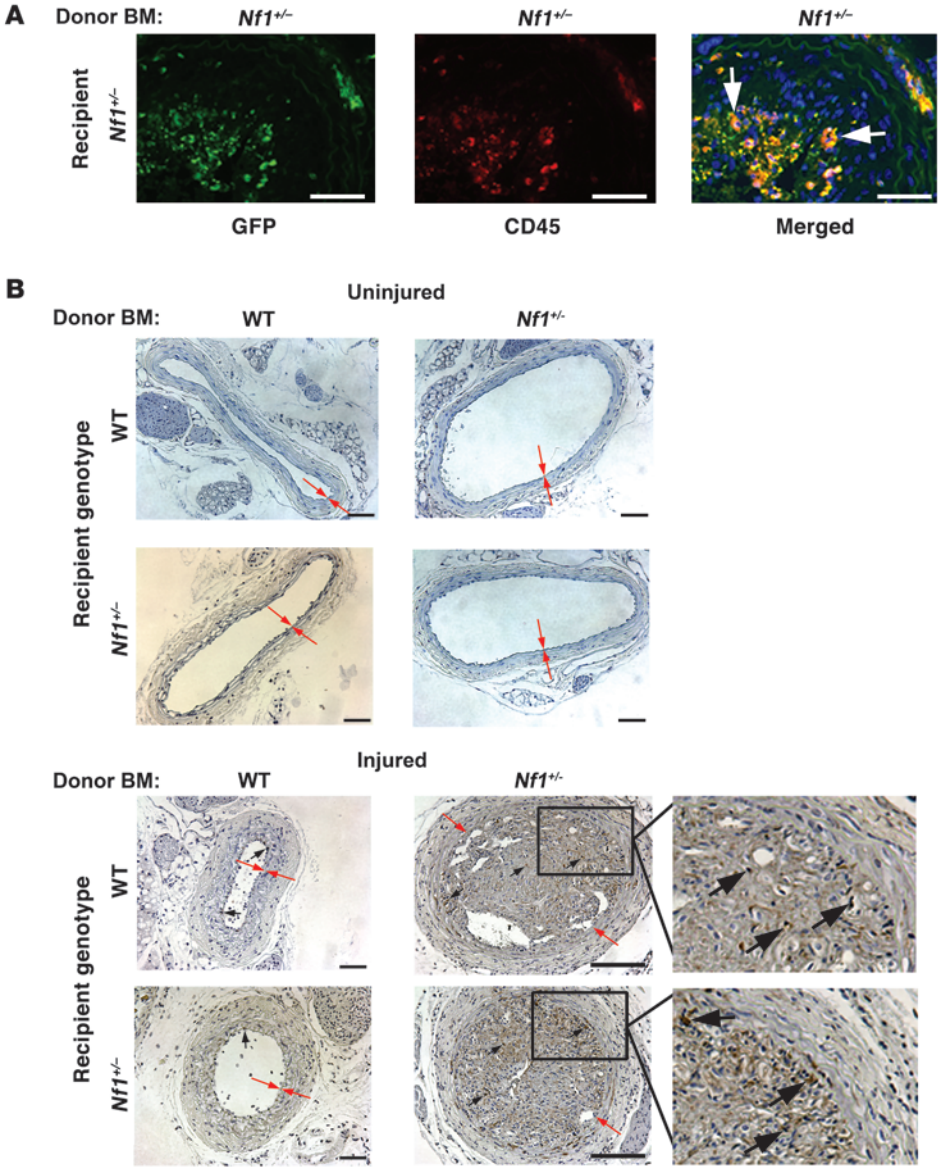

Figure 4
Identification of macrophage accumulation within the neointima of WT and *Nf1*$^{+/-}$ mice transplanted with WT and *Nf1*$^{+/-}$ BM. (**A**) Representative photomicrographs of injured carotid artery cross sections from *Nf1*$^{+/-}$ mice transplanted with *Nf1*$^{+/-}$ BM stained with anti-GFP (green) and anti-CD45 (red). Colocalization is shown in the right panel. Arrows indicate double staining for GFP and CD45. DAPI nuclear dye is shown in blue. Scale bars: 250 μm. (**B**) Representative photomicrographs of uninjured and injured carotid artery cross sections from WT and *Nf1*$^{+/-}$ mice transplanted with WT or *Nf1*$^{+/-}$ BM stained with anti-Mac3 antibody (brown) and counterstained with hematoxylin (blue). Red arrows indicate neointima boundaries. Black boxes identify area of injured artery that is magnified in the far-right lower panels. Black arrows represent positive Mac3 staining. Scale bars: 50 μm. Original magnification of far-right panels, ×400.

we utilized immunohistochemistry to identify the lineage of BMDCs within the neointima. We costained carotid artery cross sections with anti-CD45 and anti-GFP antibodies to determine whether the GFP-positive cells within the neointima were BM-derived hematopoietic cells (Figure 4A). Costaining demonstrated that all GFP-positive cells were also CD45 positive and that all hematopoietic cells within the neointima were BM derived (Figure 4A). In order to identify the hematopoietic cells within the neointima, we analyzed carotid artery cross sections utilizing specific cell surface antigens for the presence of lymphocytes, mast cells, and macrophages. Lymphocytes, mast cells, and macrophages are all inflammatory cells that secrete growth factors and cytokines that have been implicated in neointima formation (25–27). Further, our group has demonstrated that neurofibromin is a critical regulator of Ras activation in both lymphocytes and mast cells in vitro and in vivo (14, 28). Based on immunohistochemistry, lymphocytes accounted for less than 5% of the BMDCs within the neointima (data not shown), and mast cells were not present in the neointima or vessel wall of injured arteries (data not shown). However, anti-Mac3 staining of injured carotid arteries demonstrated that the majority (>80%) of the GFP- and CD45-positive cells within the neointima of all transplant groups were macrophages (Figure 4B). Immunostaining with the macrophage marker F4/80 showed a staining pattern similar to that of anti-Mac3 staining (data not shown). Consistent with the results of anti-GFP immunohistochemistry, WT and *Nf1*$^{+/-}$ mice transplanted with WT BM had minimal accumulation of macrophages within the intima area compared with WT and *Nf1*$^{+/-}$ mice reconstituted with *Nf1*$^{+/-}$ BM in response to injury (Figure 4B).

Based on this observation, we investigated whether heterozygous inactivation of *Nf1* leads to increased numbers of circulating monocytes. Peripheral blood samples were taken from uninjured WT and *Nf1*$^{+/-}$ mice, and complete blood count analysis was completed. At baseline, *Nf1*$^{+/-}$ mice had a 1.5-fold increase in the percentage of circulating monocytes compared

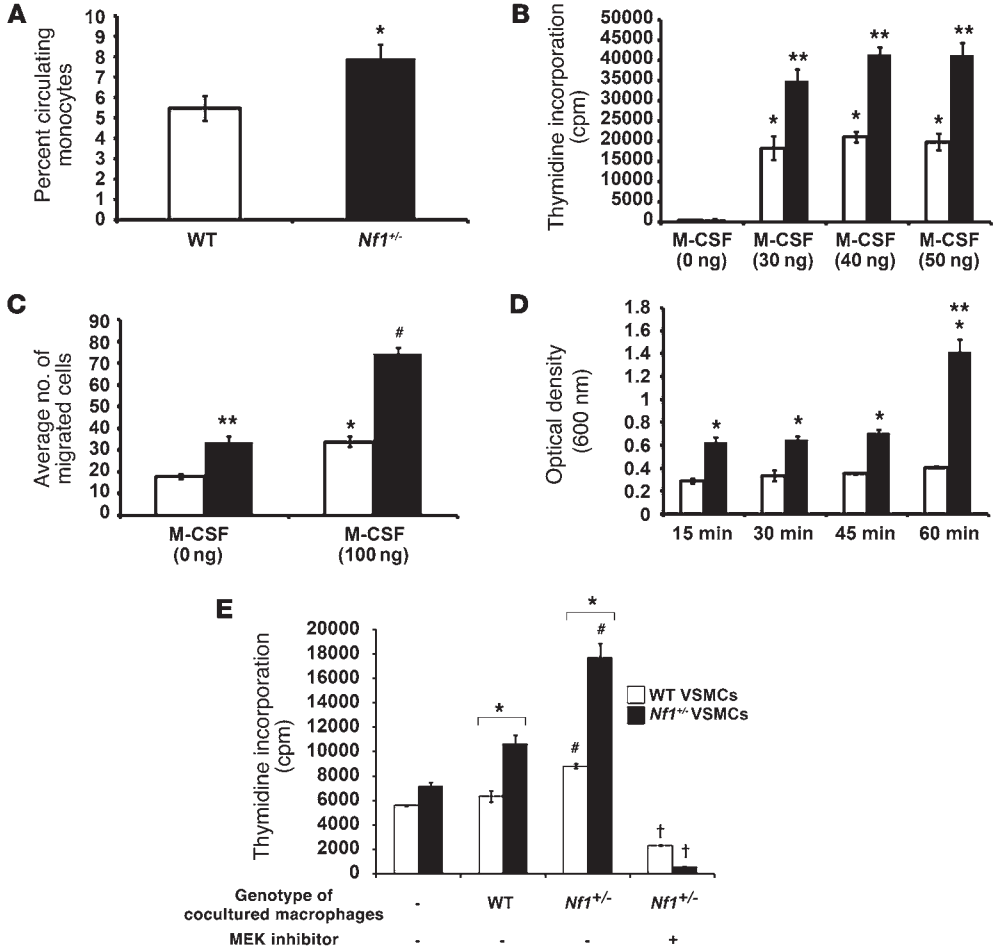

Figure 5

In vitro function of *Nf1*$^{+/-}$ macrophages. (**A**) Percent monocytes in peripheral blood of WT and *Nf1*$^{+/-}$ mice. Data represent mean percentage ± SEM, $n = 8$. $^{*}P = 0.02$ for *Nf1*$^{+/-}$ versus WT by Student's unpaired *t* test. (**B**) WT (white bars) and *Nf1*$^{+/-}$ (black bars) macrophage proliferation in response to M-CSF. Data represent mean cpm ± SEM, $n = 4$. $^{*}P < 0.001$ for unstimulated WT versus M-CSF–stimulated WT macrophages; $^{**}P < 0.001$ for M-CSF–stimulated *Nf1*$^{+/-}$ versus M-CSF–stimulated WT macrophages, by 1-way ANOVA. (**C**) WT (white bars) and *Nf1*$^{+/-}$ (black bars) macrophage haptotaxis in response to M-CSF. Data represent mean number of migrated cells ± SEM, $n = 4$. $^{*}P < 0.001$ for unstimulated WT versus M-CSF–stimulated WT macrophages; $^{**}P < 0.001$ for unstimulated WT versus unstimulated *Nf1*$^{+/-}$ macrophages; $^{\#}P < 0.001$ for unstimulated *Nf1*$^{+/-}$ versus M-CSF–stimulated *Nf1*$^{+/-}$ macrophages, by 1-way ANOVA. (**D**) WT (white bars) and *Nf1*$^{+/-}$ (black bars) macrophage adhesion to fibronectin. Data represent mean optical density ± SEM, $n = 4$. $^{*}P < 0.001$ for WT versus *Nf1*$^{+/-}$ macrophages; $^{**}P < 0.01$ for *Nf1*$^{+/-}$ macrophages at 60 minutes versus *Nf1*$^{+/-}$ macrophages at all other time points, by 1-way ANOVA. (**E**) Macrophage stimulation of WT and *Nf1*$^{+/-}$ VSMC proliferation. Data represent mean cpm ± SEM, $n = 3$. $^{*}P < 0.05$ for *Nf1*$^{+/-}$ VSMCs cocultured with WT or *Nf1*$^{+/-}$ macrophages versus WT VSMCs; $^{\#}P < 0.05$ for WT VSMCs cocultured with *Nf1*$^{+/-}$ macrophages versus WT macrophages and for *Nf1*$^{+/-}$ VSMCs cocultured with *Nf1*$^{+/-}$ macrophages versus WT macrophages; $^{\dagger}P < 0.05$ for WT and *Nf1*$^{+/-}$ VSMCs treated with MEK inhibitor versus no inhibition, by 1-way ANOVA.

with WT mice (Figure 5A). In order to determine whether neurofibromin regulates the migration, proliferation, and adhesion of macrophages, which are cellular functions critical for the recruitment and retention of macrophages in the vessel wall, we isolated and purified macrophages from the BM of *Nf1*$^{+/-}$ and WT mice. Stimulation of the macrophages with M-CSF, a growth factor critical in neointima formation, demonstrated that *Nf1*$^{+/-}$ macrophages had a 2-fold increase in proliferation (Figure 5B) and migration (Figure 5C) compared with WT macrophages. Further, *Nf1*$^{+/-}$ macrophages showed significantly increased adhesion compared with WT macrophages (Figure 5D). Consistent with increased accumulation of *Nf1*$^{+/-}$ macrophages into the neointima in vivo, these data clearly demonstrate that heterozygous inactivation of *Nf1* increases macrophage migration, proliferation, and adhesion in vitro.

To test whether *Nf1*$^{+/-}$ macrophages directly stimulate VSMC proliferation (cell-to-cell contact), we cocultured WT and *Nf1*$^{+/-}$ BM-derived macrophages with WT or *Nf1*$^{+/-}$ VSMCs. Thymidine incorporation assays in response to WT and *Nf1*$^{+/-}$ macrophage coculture revealed that *Nf1*$^{+/-}$ VSMCs had increased proliferation compared with WT VSMCs when cocultured with either WT or *Nf1*$^{+/-}$ macrophages (Figure 5E). Further, *Nf1*$^{+/-}$ VSMCs had significantly increased proliferation when cocultured with *Nf1*$^{+/-}$ compared with WT macrophages (Figure 5E). Consistent with previous

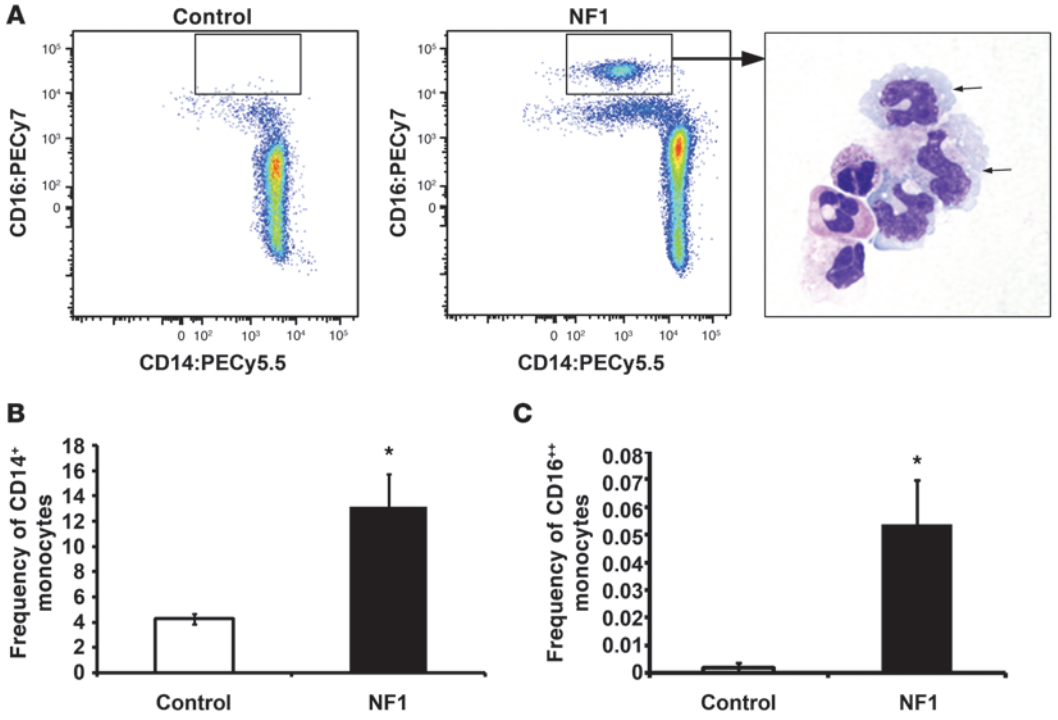

Figure 6
Identification of circulating monocytes from peripheral blood of healthy adult controls and NF1 patients. (**A**) Representative multiparameter flow cytometry analysis plot of peripheral blood monocytes identified by CD14 and CD16 cell surface expression in healthy adult controls and NF1 patients. Black box identifies the $CD14^{dim}CD16^{bright}$ monocyte population. Isolated $CD14^{dim}CD16^{bright}$ monocytes identified by May-Grünwald-Giemsa staining are shown in the far-right panel. Arrows indicate monocytes. Data represent 10 independent observations. (**B**) Quantification of the frequency of $CD45^{+}CD14^{+}$ monocytes in circulation from healthy adult control and NF1 patient peripheral blood MNCs. Data represent the mean frequency ± SEM, $n = 5$. *$P = 0.024$ by Student's unpaired t test with Welch correction. (**C**) Quantification of the frequency of $CD45^{+}CD14^{dim}CD16^{bright}$ ($CD16^{++}$) monocytes in circulation from healthy adult control and NF1 patient peripheral blood MNCs. Data represent the mean frequency ± SEM, $n = 5$. *$P = 0.0012$ by Student's unpaired t test.

studies that linked the Ras/Erk signaling pathway to the hyperproliferative phenotype of $Nf1^{+/-}$ VSMCs (9, 10, 15), treatment of the cells with the MEK inhibitor PD98509 abrogated both WT and $Nf1^{+/-}$ VSMC proliferation induced by macrophage coculture (Figure 5E). Surprisingly, increased VSMC proliferation was not observed in $Nf1^{+/-}$ VSMCs compared with WT VSMCs when stimulated with macrophage-conditioned media (data not shown), indicating that the increased VSMC proliferation is mediated through direct contact of macrophages with VSMCs. Collectively, these cellular and genetic data demonstrate that neointima formation in $Nf1^{+/-}$ mice is directly related to increased vascular inflammation and accumulation of BMDCs, especially macrophages, into the evolving neointima.

NF1 patients show evidence of chronic inflammation. Given the observation of vascular inflammation in $Nf1^{+/-}$ mice, we tested whether NF1 patients show cellular and cytokine evidence of vascular inflammation by assaying for previously established biomarkers linked to human vasoocclusive disease (29–31). Utilizing multiparameter flow cytometry, we analyzed MNCs isolated from the peripheral blood of NF1 patients (37.6 ± 9.7 years) and age- and sex-matched healthy controls (40.2 ± 8.1 years) for inflammatory monocyte populations. The frequency of total circulating monocytes was initially determined by assaying total MNCs for monocytes that coexpressed the cell surface antigens CD45 and CD14 (32). NF1 patients had markedly increased frequencies of circulating monocytes compared with healthy controls (Figure 6A). We further measured specific circulating monocyte populations to identify proinflammatory monocytes, which coexpress CD14 and CD16 ($CD14^{+}CD16^{+}$) (33). Proinflammatory monocytes have been identified in the peripheral blood of patients with coronary artery disease and atherosclerosis (30, 34). Analysis of NF1 patient peripheral blood monocytes identified a population of cells that had increased CD16 expression ($CD14^{dim}CD16^{bright}$) compared with the traditional $CD14^{+}CD16^{+}$ monocytes, a population that was not observed in peripheral blood samples from healthy controls (Figure 6, B and C). Based on the side scatter profile, the population of $CD14^{dim}CD16^{bright}$ monocytes, isolated from NF1 patients, was larger in size than other monocyte populations, indicating the cells had increased granularity, a characteristic of monocyte activation (35). Further, May-Grünwald-Giemsa staining of the isolated $CD14^{dim}CD16^{bright}$ monocytes demonstrated that the cells were monocytes characterized by an extended cytoplasm and cytoplasmic vacuoles (Figure 6A).

Proinflammatory monocytes produce numerous inflammatory cytokines and chemokines that have been implicated in neointima formation (30, 33). Therefore, based on the increased levels of circulating monocytes and the presence of an activated

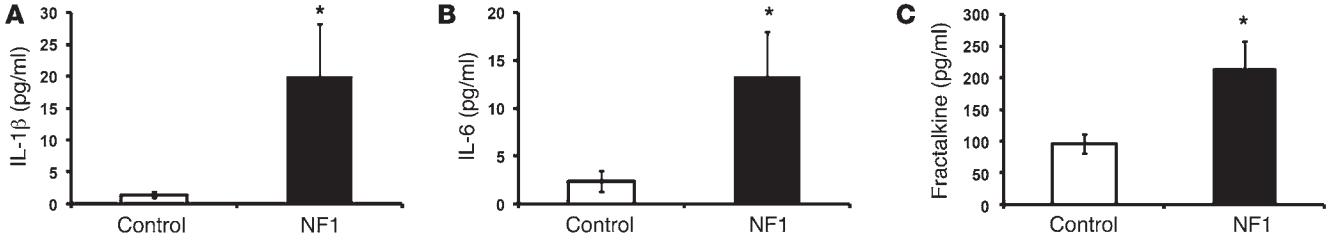

Figure 7

Analysis of inflammatory cytokines and chemokines from NF1 patient and healthy control plasma. Determination of cytokine levels in plasma isolated from control peripheral blood and NF1 patient peripheral blood. (**A**) IL-1β levels. Data represent the mean pg/ml ± SEM, $n = 6$. *$P = 0.014$ by Mann-Whitney *U* test. (**B**) IL-6 levels. Data represent the mean pg/ml ± SEM, $n = 6$. *$P = 0.046$ by Student's unpaired *t* test of log-transformed data. (**C**) Fractalkine levels. Data represent the mean pg/ml ± SEM, $n = 6–8$. *$P = 0.0393$ by Student's unpaired *t* test with Welch correction.

monocyte population, we hypothesized that NF1 patients would also have increased levels of inflammatory cytokines and chemokines in their peripheral blood, a correlation that has been made in other patient populations with the progression of vascular disease (36–38). We analyzed plasma samples from NF1 patients and healthy controls for the presence of the specific proinflammatory cytokines IL-1β and IL-6. Analysis of plasma samples from NF1 patients with no known vascular disease (17 ± 2 years, $n = 6$) and healthy controls (18.5 ± 3.4 years, $n = 7$) showed significantly elevated levels of IL-1β and IL-6 in the plasma samples from NF1 patients compared with controls (Figure 7). The production of proinflammatory cytokines has been linked to the activation of the endothelium and increased expression of chemokines involved in the recruitment of monocytes to the vessel wall (39, 40). Interestingly, NF1 patient plasma samples had significantly elevated levels of soluble fractalkine (Figure 6), an adhesion molecule expressed on inflamed endothelium that is involved in rapid, high-affinity binding of monocytes (40, 41). The increased number of circulating monocytes and production of inflammatory cytokines provide direct evidence of chronic inflammation in NF1 and elevation of biomarkers previously identified as critical risk factors in other patient populations with vascular disease reminiscent of NF1 vasculopathy.

Discussion

Vascular disease is one of the least understood complications of NF1, even though it contributes to excess morbidity and mortality among younger patients (5, 6). A limiting factor in understanding NF1 vasculopathy was the lack of an in vivo model that mimics the human disease. We previously demonstrated that mechanical arterial injury results in increased Ras activation and VSMC proliferation in the emerging neointima of *Nf1*$^{+/-}$ mice, leading to vessel occlusive disease, reminiscent of NF1 vasculopathy (10). Further, we demonstrated that neointima formation in *Nf1*$^{+/-}$ mice was completely abrogated by the administration of imatinib mesylate, a pharmacological inhibitor of both the PDGFβ receptor (PDGFβ-R) and C-kit receptor (10). This observation identified a potential mechanism through which inhibition of PDGF induced VSMC proliferation and/or recruitment of BMDCs via C-kit activation would abrogate neointima formation in *Nf1*$^{+/-}$ mice. These results are important given that hyperactive Ras signaling through either the PDGFβ-R or C-kit receptor accelerates vascular disease (42). Therefore, based on these observations, experiments were designed in the current study to specifically identify which cell lineages were critical for neointima formation in vivo.

The endothelium functions as a barrier between the VSMCs within the vessel wall and the blood, controlling the transmigration of circulating cells into the vessel and inhibiting the proliferation and migration of VSMCs within the vessel wall (43, 44). Endothelial dysfunction by inflammatory activation upregulates the expression of adhesion molecules on the surface of the endothelium, recruiting circulating inflammatory cells to the vessel wall (39, 43, 45, 46). Vascular inflammation, defined as the infiltration of inflammatory cells into the vessel wall, has been described in atherosclerosis and in vivo models of neointima formation (24, 34). Endothelial dysfunction is one of the first steps in vascular inflammation, initiating a cascade of events that, if unchecked, result in vascular lesion formation (11, 47). Although neurofibromin is a known critical regulator of Ras activation in ECs, VSMCs, and BMDCs (14–16, 28), it remains unclear whether endothelial dysfunction, hyperproliferation or migration of VSMCs, or increased activation of circulating BMDCs is the predominant factor in neointima formation in *Nf1*$^{+/-}$ mice. Therefore, we interrogated the role of heterozygous inactivation of *Nf1* in ECs, VSMCs, and BMDCs in neointima formation.

In this study, we demonstrated that heterozygous inactivation of *Nf1* in ECs or VSMCs alone was insufficient to recapitulate the enhanced neointima formation observed in *Nf1*$^{+/-}$ mice in response to carotid ligation. Morphometric analysis showed that WT, *Nf1*$^{fl/+}$*;Tie2cre*, and *Nf1*$^{fl/+}$*;SM22cre* mice had similar neointima formation in response to ligation, and levels in these genotypes were significantly lower than those in *Nf1*$^{+/-}$ mice. Although *cre* expression in the *Nf1*$^{fl/+}$*;Tie2cre* mice was not limited to the ECs and some partial recombination was observed in the BM cells of the *Nf1*$^{fl/+}$*;Tie2cre* mice, this is insufficient to promote neointima formation in response to injury. The transplant experiments described in this report definitively demonstrate that heterozygous inactivation of *Nf1* in BMDCs alone is sufficient for neointima formation in response to vascular injury. Specifically, we showed that both WT and *Nf1*$^{+/-}$ mice reconstituted with *Nf1*$^{+/-}$ BMDCs had enhanced neointima formation characterized by an accumulation of BMDCs in response to carotid ligation. Immunohistochemistry demonstrated that greater than 80% of the *Nf1*$^{+/-}$ BMDCs within the neointima were macrophages. Through in vitro studies, we discovered that heterozygous inactivation of *Nf1* in macrophages resulted in increased proliferation, migration, and adhesion compared with WT controls. Further, we demonstrated that direct contact of macrophages with *Nf1*$^{+/-}$ VSMCs is required to stimulate proliferation through a Ras/Erk-dependent pathway in vitro. These studies identify *Nf1*$^{+/-}$ BMDCs as necessary and sufficient

for neointima formation and describe what we believe to be a new role for neurofibromin as an important regulator of macrophage function in vivo and in vitro. Further, these data provide a paradigm according to which infiltration of inflammatory cells is the major determinant of vessel occlusion despite the role of neurofibromin in regulating EC and VSMC function.

The accumulation of macrophages in the vessel wall in response to arterial injury suggests that inflammation makes a direct contribution to neointima formation in *Nf1*$^{+/-}$ mice. Macrophages play an important role in neointima formation through the production of growth factors and cytokines that activate ECs and stimulate VSMC migration and proliferation (48, 49). Further, macrophages are a potent source of matrix proteases (50), which cleave collagen within the vessel wall, resulting in matrix remodeling and allowing VSMCs to migrate from the media into the intima in response to chemotactic agents generated by arterial injury (51, 52). It has previously been reported that cellular proliferation is drastically reduced after 2 weeks following injury, although the neointima continues to develop due to the accumulation and remodeling of matrix (22, 53). The continued growth of the neointima in the absence of VSMC proliferation suggests a mechanism by which the WT mice transplanted with *Nf1*$^{+/-}$ BM had neointima formation equivalent to that of *Nf1*$^{+/-}$ mice transplanted with *Nf1*$^{+/-}$ BM 28 days after injury, despite the observation that *Nf1*$^{+/-}$ mice had significantly more BMDCs within the neointima. Further, these observations suggest that *Nf1*$^{+/-}$ vascular cells promote accumulation and survival of *Nf1*$^{+/-}$ BMDCs within the neointima. The observations are consistent with other reports in NF1 that provide evidence to support the role of an *Nf1* haploinsufficient microenvironment in clinical manifestations of the disease (54, 55). Based on the current experimental results, we are now dissecting the mechanism of macrophage facilitation of neointima formation utilizing hematopoietic cell–specific *cre* mice to ablate the *Nf1* gene in different blood cell types and murine models deficient in various macrophage functions.

Inflammation is linked to vascular disease in patient populations including atherosclerosis and coronary artery disease (29, 34). In this study, we determined that NF1 patients with no overt vascular cardiovascular disease have increased numbers of circulating monocytes compared with healthy controls. Further, we identified a population of monocytes in NF1 patients that is characteristic of an activated state, including increased CD16 expression and increased size (35). The finding of increased levels of the proinflammatory cytokines IL-1β and IL-6 in plasma samples from NF1 patients supports the observation that NF1 patients have increased activated monocytes in circulation, given that, in peripheral blood, monocytes are the main producers of IL-1β and IL-6 (56). Along with endothelial activation, cytokines have been described to affect arterial endothelium-dependent vasodilation. Iversen et al. demonstrated that the cytokines TNF-α, IL-6, and IL-10 induced arterial contraction in an endothelium-dependent manner (57). In preliminary studies, NF1 patients showed decreased endothelium-dependent dilation compared with normal standards, with no difference detected in smooth muscle–dependent dilation. An important observation in this study was that reduced endothelium-dependent dilation was observed in NF1 patients with no known vascular disease (J.M. Friedman, unpublished observations). We are currently conducting studies to determine the incidence of subclinical vascular disease in NF1 patients, along with identifying potential biomarkers that correlate to the progression of vascular disease in patients.

Further, in this report, we demonstrated that NF1 patients have increased levels of soluble fractalkine in circulation. Membrane-bound fractalkine is an adhesion molecule expressed on an inflamed endothelium when activated by proinflammatory cytokines, such as TNF-α and IL-1β (31, 58). Fractalkine produces a high-affinity interaction with CX3CR1-expressing cells, including inflammatory monocytes, that allows cells to rapidly bind to the endothelium under normal flow conditions (40, 41, 59). Fractalkine is cleaved from the cell membrane, resulting in soluble fractalkine, which functions as a potent chemoattractant for monocytes (58), and the inflammatory CD14^{+}CD16^{+} monocytes have been demonstrated to preferentially express CX3CR1 (60). In vivo, arterial injury upregulated the expression of fractalkine, and genetic ablation of *Cx3cr1* abrogates neointima formation through impaired monocyte recruitment (61). Taken together, the data indicate that upregulation of fractalkine expression in NF1 patients in response to increased inflammatory cytokines would result in increased recruitment and attachment of monocytes to the vessel wall, leading to endothelial dysfunction and subsequent vascular disease.

In this report, we determined that heterozygous inactivation of *Nf1* in BMDCs is necessary and sufficient for neointima formation in response to arterial ligation. The neointima of mice reconstituted with *Nf1*$^{+/-}$ BM was characterized by an accumulation of macrophages, while mice transplanted with WT BM showed minimal neointima formation. These observations demonstrate that neurofibromin is a regulator of macrophage function and that vascular inflammation is a critical factor in neointima formation. Further, the increased levels of circulating monocytes and increased expression in inflammatory cytokines observed in NF1 patients provide evidence of chronic inflammation associated with NF1. In sum, these studies provide the first genetic and cellular evidence to our knowledge of vascular inflammation in *Nf1*$^{+/-}$ mice and NF1 patients and provide a framework for understanding the pathogenesis of NF1 vasculopathy and potential therapeutic and diagnostic interventions in future studies.

Methods

Animals. All protocols for this study were approved by the Indiana University Laboratory Animal Research Center. *Nf1*$^{+/-}$ mice were obtained from Tyler Jacks (Massachusetts Institute of Technology, Cambridge) and backcrossed 13 generations into the C57BL/6J strain. The *Nf1* allele was genotyped as previously described (62). *Nf1*$^{fl/fl}$ mice were obtained from Luis Parada (University of Texas Southwestern Medical Center, Dallas) and backcrossed 13 generations into the 129SvJ strain and genotyped as previously described (63). GFP (stock 3291) (64), *SM22cre* (stock 4746), and *Tie2cre* (stock 4128) mice were purchased from The Jackson Laboratory and maintained on the C57BL/6 strain. *Nf1*$^{fl/fl}$ mice were crossed with either *SM22cre* or *Tie2cre* mice to generate C57BL/6 × 129SvJ pups. *Nf1*$^{fl/+}$*; SM22cre* and *Nf1*$^{fl/+}$*;Tie2cre* mice were used for experiments. Genotype was confirmed by identification of *cre* by PCR according to Jackson Laboratory protocols. Cre-mediated recombination was confirmed by PCR as previously described (63). *Nf1*$^{+/-}$ and WT controls were generated by crossing *Nf1*$^{fl/fl}$ 129SvJ mice with *Nf1*$^{+/-}$ C57BL/6 mice. *Nf1*$^{+/-}$ mice that ubiquitously express GFP were generated by crossing GFP WT mice with *Nf1*$^{+/-}$ mice. Only male mice, at least 12 weeks of age, were used for experiments.

Carotid artery ligation. In 3 independent experiments, carotid artery injury was induced by complete ligation of the left common carotid artery as previously described (22). Briefly, mice were anesthetized by inhalation of an isoflurane (2%)/oxygen (98%) mixture. Under a dissecting scope (Leica), the entire left carotid artery was exposed through a midline incision of the

neck. The common carotid artery was ligated just proximal to the bifurcation using a 6-O silk suture (Fine Science Tools). Mice recovered for 28 days with no sign of stroke or complication.

BM transplantation. Femurs and tibias from WT and *Nf1*$^{+/-}$ mice that ubiquitously expressed GFP were flushed with Iscove's modified Dulbecco's medium (IMDM; Invitrogen). Male, 12-week-old recipient WT and *Nf1*$^{+/-}$ mice were conditioned by lethal irradiation (11 Gy). Unfractionated BM cells (5×10^6 cells) were injected via tail vein into conditioned recipients. After a 4-month reconstitution period, peripheral blood was collected via tail vein bleeding to determine percent engraftment. Red blood cells were lysed (QIAGEN), and MNCs were resuspended and analyzed by flow cytometry using FACSCalibur (BD); data were analyzed using FlowJo software (Tree Star). Only mice with greater than 85% engraftment were used for experiments.

Histopathology and immunohistochemistry. Twenty-eight days after ligation, whole ligated and contralateral uninjured carotid arteries were harvested from mice. Mice were anesthetized with 1.25% Avertin (Sigma-Aldrich) and were perfusion fixed at constant pressure (100 mmHg) with 0.9% sodium chloride followed by Z-fix solution (Anatech). Under a dissecting scope, carotid arteries were excised, then fixed overnight at 4°C in Z-fix solution and paraffin embedded. Serial 5-μm arterial cross sections were made every 200 μm across the length of the carotid artery. H&E staining was performed according to standard methods (Anatech).

For immunohistochemistry, paraffin-embedded sections were dewaxed followed by enzymatic (20 μg/ml Proteinase K; Roche) antigen retrieval. Sections were blocked with Protein Block (Dako) and were incubated with anti-GFP (1:1,000; Abcam) or anti-Mac3 (1:50; BD Biosciences — Pharmingen) primary antibodies. Sections were incubated with the appropriate secondary antibody (Vector Laboratories) and visualized by 3,3′-diaminobenidine (DAB; Vector Laboratories) and counterstained with hematoxylin.

For immunofluorescence costaining, paraffin-embedded sections were dewaxed, followed by enzymatic antigen retrieval. Sections were blocked with M.O.M. reagents according to the manufacturer's recommendations (Vector Laboratories) and incubated with anti-GFP (1:1,000; Abcam) primary antibody followed by the appropriate biotinylated secondary antibody. The sections were then coincubated with anti–α-SMA (1:400; Sigma-Aldrich) and Alexa Fluor 546 streptavidin–conjugated antibody (BD Pharmingen) and mounted with ProLong Gold antifade mounting media containing 6-diamidino-2-phenylindole dihydrochloride (Invitrogen).

Morphometric analysis. H&E-stained arterial cross sections 400, 800, and 1,200 μm proximal to the ligation were analyzed for neointima formation using Metamorph 6.1 (Universal Imaging Systems Corp.). Lumen area, area inside the internal elastic lamina (IEL), and area inside the external elastic lamina (EEL) were measured for each cross section. Intima area was calculated by subtracting the lumen area from the IEL area, and the media area was calculated by subtracting the IEL area from the EEL area. I/M ratio was calculated as intima area divided by media area as previously described (22).

Isolation of BM-derived macrophages. BM-derived macrophages were generated from femurs, tibias, and iliac crest of 8- to 12-week-old WT and *Nf1*$^{+/-}$ mice. Briefly, BM cells were flushed into a 50-ml Falcon tube using syringe-needle and IMDM. Cells were collected by centrifugation at 800 *g* for 5 minutes (Beckman Coulter) at room temperature, and rbc were lysed with rbc lysis buffer for 5 minutes at room temperature. The cells were centrifuged and resuspended in 5 ml IMDM. Low-density BM cells were isolated by density gradient centrifugation using Histopaque 1083 (Sigma-Aldrich). For macrophages, low-density BM cells were cultured in complete media consisting of IMDM, 20% FBS supplemented with 1% penicillin/streptomycin, and 100 ng/ml M-CSF (PeproTech). Cells were used for experiments between 3 and 6 passages.

Macrophage proliferation assay. Proliferation was assessed by incorporation of radioactive thymidine in WT and *Nf1*$^{+/-}$ BM-derived macrophages. Briefly, cells were starved in media containing 0.2% BSA in IMDM without growth factors for 6–7 hours. Macrophages (5×10^4 cells) were placed in a 96-well plate in 200 μl starvation media in either the absence or presence of the indicated concentration of M-CSF. Cells were cultured for 48 hours and subsequently pulsed with 1.0 μCi (0.037 MBq) [^{3}H]thymidine for 6 hours. Cells were harvested using an automated 96-well cell harvester (Brandel), and thymidine incorporation was determined as counts per minute (cpm).

Macrophage migration assay. Haptotactic cell migration assay was performed as previously described (65). Briefly, the bottom of Transwell filters (8-μM pore filter; Costar) were coated with 20 μg/ml fibronectin CH296 peptide for 2 hours at 37°C and rinsed twice with PBS containing 2% BSA. The fibronectin CH296 peptide–coated filters were placed in the lower chamber containing 500 μl complete medium with or without M-CSF (100 ng/ml). Macrophages (2.5×10^5 cells) were resuspended in 100 μl IMDM and allowed to migrate toward the bottom of the top chamber. After 20 hours of incubation at 37°C, nonmigrated cells in the upper chamber were removed with a cotton swab. The migrated cells that attached to the bottom surface of the membrane were stained with 0.1% crystal violet dissolved in 0.1 M borate, pH 9.0, and 2% ethanol for 5 minutes at room temperature. The number of migrated cells per membrane was determined in 10 random fields with an inverted microscope using a 20× objective lens.

Macrophage adhesion assay. Adhesion assay was performed as previously described (65). Briefly, flat-bottom 96-well polystyrene plates (BD Biosciences) were coated with 20 μg/ml fibronectin fragment CH296 in PBS for 1 hour at 37°C. Wells were washed once with PBS, incubated with 20 mg/ml heat-inactivated BSA for 1 hour at 37°C to block nonspecific sites, and again washed twice with PBS. For examination of cell adhesion on the coated surface, 1×10^5 cells were added to each well and incubated at 37°C for different time intervals (15 minutes, 30 minutes, 45 minutes, and 1 hour). At the end of the incubation, unbound cells were removed by aspiration, and wells were washed twice with cold PBS. Adherent cells were fixed with 3.5% formaldehyde and stained with 0.1% crystal violet. The stain was eluted with 10% acetic acid, and absorbance was determined at 600 nm using a microplate reader (Spectramax 250; Molecular Devices).

VSMC and macrophage coculture proliferation assay. VSMCs were obtained and cultured as previously described (15), and BM macrophages were isolated and cultured as described above. VSMCs were plated at a density of 3,500 cells/cm^2 and deprived of growth factors for 24 hours. Macrophages, at a density of 1,750 cells/cm^2 were added to the quiescent VSMCs for 24 hours at 37°C, 5% CO_2. At the end of the coincubation period, collagenase (1 mg/ml) was used to remove the macrophages from the VSMC culture. VSMCs were pulse labeled with 1 μCi/ml of tritiated thymidine (PerkinElmer) for 24 hours, and β emission was measured (Beckman Coulter) as previously described (15). Where stated, VSMCs were preincubated with 50 μM PD98509 30 minutes before the addition of macrophages to the culture.

Patient recruitment. NF1 patients were recruited through the Indiana University Neurofibromatosis Clinic at Riley Hospital for Children. All patients had a medical history and physical examination performed to confirm the diagnosis of NF1 using standard NIH clinical criteria (66). Patients with a personal history of cancer or currently using anticancer drugs or patients who were pregnant were excluded from the study. All patients gave informed consent prior to their participation in the study.

Polychromatic flow cytometric analysis of peripheral blood MNCs. Blood samples were collected from NF1 patients (37.6 ± 9.7 years) and age- and sex-matched healthy controls (40.2 ± 8.1 years) into EDTA Vacutainer tubes (BD Biosciences). MNCs were isolated from 16 ml of peripheral blood by density centrifugation using Ficoll-Paque Plus (GE Healthcare) as previously described (67). A total of 1×10^6 MNCs were resuspended in PBS with 2% FBS and incubated with human FcR Blocking Reagent (Miltenyi

Biotec) for 10 minutes at 4°C. After blocking, MNCs were incubated for 30 minutes at 4°C with the following primary conjugated monoclonal antibodies: anti–human CD14–PECy5.5 (Abcam), anti–human CD45–allophycocyanin–Alexa Fluor 750 (Invitrogen), and anti–human CD16–PECy7 (BD Biosciences — Pharmingen), as well as the live/dead marker ViVid (Invitrogen). After staining, MNCs were washed 2 times with PBS with 2% FBS and fixed in 1% formaldehyde (Sigma-Aldrich) for a minimum of 24 hours. Stained MNC samples were acquired on a BD LSRII flow cytometer equipped with a 405-nm violet laser, 488-nm blue laser, and 633-nm red laser. At least 300,000 events were collected for each sample. Data were collected uncompensated and analyzed using FlowJo software version 8.7.3 (Tree Star). The Institutional Review Board of the Indiana University School of Medicine approved all protocols.

Quantification of cytokines in patient plasma samples. Blood samples were collected from NF1 patients (17 ± 2 years, $n = 6$) and healthy age-matched controls (18.5 ± 3.4 years, $n = 7$) into EDTA Vacutainer tubes (BD Biosciences). Plasma was isolated from 3 ml of blood by centrifugation at 900 *g* for 10 minutes at 4°C. Plasma was aliquoted and stored at –80°C until use. IL-1β, IL-6, IL-10, TNF-α, GM-CSF, MCP-1, IFN-γ, and fractalkine were quantified by using a custom Milliplex Cytokine kit (Millipore) according to the manufacturer's recommendations. Only plasma samples that had not undergone a freeze/thaw cycle were analyzed. Samples were analyzed by a Luminex 200 version 2.3 (Millipore), and StatLIA Immunoassay Analysis Software (Brendan Technologies Inc.) with a 5-parameter logistic curve fitting method was used to calculate sample concentrations. Concentrations below the minimum detectable concentration were set equal to the minimum detectable concentration. The Institutional Review Board of the Indiana University School of Medicine approved all protocols.

Statistics. All values are presented as mean ± SEM. All statistical analyses were performed using GraphPad InStat version 3.00 (GraphPad Software). Neointima area and I/M ratio were assessed by 1-way ANOVA with a Tukey's post-hoc test. Total number of GFP-positive cells was assessed by One-way ANOVA with Tukey's post-hoc test. Percentages of circulating monocytes and macrophage proliferation, migration, and adhesion were assessed by 2-tailed Student's unpaired *t* test. Frequency of circulating $CD45^+CD14^+$ and $CD16^{bright}CD14^+$ monocytes was assessed by 2-tailed Student's unpaired *t* test. IL-1β levels were assessed by Mann-Whitney *U* test due to unequal distribution. IL-6 levels were log transformed for equal distribution and assessed by 2-tailed Student's unpaired *t* test. Fractalkine levels were assessed by 2-tailed Student's unpaired *t* test with Welch correction. *P* values less than 0.05 were considered significant.

Acknowledgments

We thank Janice Walls for expert administrative assistance in preparation of the manuscript. This work was supported by the following grants: NIH P50 NS052606 (to D.A. Ingram Jr.) and NIH R01 HL060714 (to S.J. Conway), Department of Defense NF073122 (to D.A. Ingram Jr. and S.J. Conway), American Heart Association grant AHA-8156237 (to E. Lasater and D.A. Ingram Jr.). The project was supported by a Project Development Team within the Indiana Clinical and Translational Sciences Institute NIH/NICRR grant number RR025761.

Received for publication October 14, 2009, and accepted in revised form January 6, 2010.

Address correspondence to: David A. Ingram Jr., Herman B. Wells Center for Pediatric Research, Indiana University School of Medicine, 1044 W. Walnut St. R4/470, Indianapolis, IN 46202. Phone: 317.278.8245; Fax: 317.274.8679; E-mail: dingram@iupui.edu.

1. Riccardi VM. Neurofibromatosis: past, present, and future. *N Engl J Med*. 1991;324(18):1283–1285.
2. Viskochil D, et al. Deletions and a translocation interrupt a cloned gene at the neurofibromatosis type 1 locus. *Cell*. 1990;62(1):187–192.
3. Rasmussen SA, Friedman JM. NF1 gene and neurofibromatosis 1. *Am J Epidemiol*. 2000;151(1):33–40.
4. Ward BA, Gutmann DH. Neurofibromatosis 1: from lab bench to clinic. *Pediatr Neurol*. 2005; 32(4):221–228.
5. Friedman JM, et al. Cardiovascular disease in neurofibromatosis 1: report of the NF1 Cardiovascular Task Force. *Genet Med*. 2002;4(3):105–111.
6. Rasmussen SA, Yang Q, Friedman JM. Mortality in neurofibromatosis 1: an analysis using U.S. death certificates. *Am J Hum Genet*. 2001;68(5):1110–1118.
7. Rosser TL, Vezina G, Packer RJ. Cerebrovascular abnormalities in a population of children with neurofibromatosis type 1. *Neurology*. 2005;64(3):553–555.
8. Hamilton SJ, Friedman JM. Insights into the pathogenesis of neurofibromatosis 1 vasculopathy. *Clin Genet*. 2000;58(5):341–344.
9. Xu J, Ismat FA, Wang T, Yang J, Epstein JA. NF1 regulates a Ras-dependent vascular smooth muscle proliferative injury response. *Circulation*. 2007; 116(19):2148–2156.
10. Lasater EA, et al. Nf1+/– mice have increased neointima formation via hyperactivation of a Gleevec sensitive molecular pathway. *Hum Mol Genet*. 2008; 17(15):2336–2344.
11. Kofler S, Nickel T, Weis M. Role of cytokines in cardiovascular diseases: a focus on endothelial responses to inflammation. *Clin Sci (Lond)*. 2005;108:205–213.
12. Szmitko PE, et al. New markers of inflammation and endothelial cell activation: part I. *Circulation*. 2003; 108(16):1917–1923.
13. Ingram DA, et al. Hyperactivation of $p21^{ras}$ and the hematopoietic-specific Rho GTPase, Rac2, cooperate to alter the proliferation of neurofibromin deficient mast cells *in vivo* and *in vitro*. *J Exp Med*. 2001;194(1):57–70.
14. Ingram DA, et al. Genetic and biochemical evidence that haploinsufficiency of the *Nf1* tumor suppressor gene modulates melanocyte and mast cell fates *in vivo*. *J Exp Med*. 2000;191(1):181–188.
15. Li F, et al. Neurofibromin is a novel regulator of RAS-induced signals in primary vascular smooth muscle cells. *Hum Mol Genet*. 2006;15(11):1921–1930.
16. Munchhof AM, et al. Neurofibroma-associated growth factors activate a distinct signaling network to alter the function of neurofibromin-deficient endothelial cells. *Hum Mol Genet*. 2006; 15(11):1858–1869.
17. Kisanuki YY, et al. Tie2-Cre transgenic mice: a new model for endothelial cell-lineage analysis in vivo. *Dev Biol*. 2001;230(2):230–242.
18. Holtwick R, et al. Smooth muscle-selective deletion of guanylyl cyclase-A prevents the acute but not chronic effects of ANP on blood pressure. *Proc Natl Acad Sci U S A*. 2002;99(10):7142–7147.
19. Gitler AD, et al. Nf1 has an essential role in endothelial cells. *Nat Genet*. 2003;33(1):75–79.
20. Iwama A, et al. Molecular cloning and characterization of mouse TIE and TEK receptor tyrosine kinase genes and their expression in hematopoietic stem cells. *Biochem Biophys Res Commun*. 1993; 195(1):301–309.
21. Schlaeger TM, et al. Uniform vascular-endothelial-cell-specific gene expression in both embryonic and adult transgenic mice. *Proc Natl Acad Sci U S A*. 1997; 94(7):3058–3063.
22. Kumar A, Lindner V. Remodeling with neointima formation in the mouse carotid artery after cessation of blood flow. *Arterioscler Thromb Vasc Biol*. 1997; 17(10):2238–2244.
23. Kuhel DG, Zhu B, Witte DP, Hui DY. Distinction in genetic determinants for injury-induced neointimal hyperplasia and diet-induced atherosclerosis in inbred mice. *Arterioscler Thromb Vasc Biol*. 2002;22(6):955–960.
24. Simon DI, Dhen Z, Seifert P, Edelman ER, Ballantyne CM, Rogers C. Decreased neointimal formation in Mac-1(–/–) mice reveals a role for inflammation in vascular repair after angioplasty. *J Clin Invest*. 2000;105(3):293–300.
25. Chamberlain J, et al. Interleukin-1beta and signaling of interleukin-1 in vascular wall and circulating cells modulates the extent of neointima formation in mice. *Am J Pathol*. 2006;168(4):1396–1403.
26. Libby P, Shi GP. Mast cells as mediators and modulators of atherogenesis. *Circulation*. 2007; 115(19):2471–2473.
27. Murayama H, et al. Deficiency of tumour necrosis factor-alpha and interferon-gamma in bone marrow cells synergistically inhibits neointimal formation following vascular injury. *Cardiovasc Res*. 2008;80(2):175–180.
28. Ingram DA, et al. Lymphoproliferative defects in mice lacking the expression of neurofibromin: functional and biochemical consequences of Nf1 deficiency in T-cell development and function. *Blood*. 2002;100(10):3656–3662.
29. Libby P, Ridker PM, Maseri A. Inflammation and atherosclerosis. *Circulation*. 2002;105(9):1135–1143.
30. Schlitt A, et al. CD14+CD16+ monocytes in coronary artery disease and their relationship to serum TNF-alpha levels. *Thromb Haemost*. 2004;92(2):419–424.
31. Umehara H, Bloom ET, Okazaki T, Nagano Y, Yoshie O, Imai T. Fractalkine in vascular biology: from basic research to clinical disease. *Arterioscler Thromb Vasc Biol*. 2004;24(1):34–40.
32. Todd RF 3rd, Van Agthoven A, Schlossman SF, Terhorst C. Structural analysis of differentiation antigens Mo1 and Mo2 on human monocytes.

Hybridoma. 1982;1(3):329–337.
33. Grage-Griebenow E, Flad HD, Ernst M. Heterogeneity of human peripheral blood monocyte subsets. *J Leukoc Biol*. 2001;69(1):11–20.
34. Hansson GK. Inflammation, atherosclerosis, and coronary artery disease. *N Engl J Med*. 2005; 352(16):1685–1695.
35. Abel PM, et al. Heterogeneity of peripheral blood monocyte populations in human immunodeficiency virus-1 seropositive patients. *FEMS Microbiol Immunol*. 1992;5(5–6):317–323.
36. Cesari M, et al. Inflammatory markers and onset of cardiovascular events: results from the Health ABC study. *Circulation*. 2003;108(19):2317–2322.
37. Lindmark E, Diderholm E, Wallentin L, Siegbahn A. Relationship between interleukin 6 and mortality in patients with unstable coronary artery disease: effects of an early invasive or noninvasive strategy. *JAMA*. 2001;286(17):2107–2113.
38. Luc G, et al. C-reactive protein, interleukin-6, and fibrinogen as predictors of coronary heart disease: the PRIME Study. *Arterioscler Thromb Vasc Biol*. 2003; 23(7):1255–1261.
39. Davies MJ, et al. The expression of the adhesion molecules ICAM-1, VCAM-1, PECAM, and E-selectin in human atherosclerosis. *J Pathol*. 1993; 171(3):223–229.
40. Fong AM, et al. Fractalkine and CX3CR1 mediate a novel mechanism of leukocyte capture, firm adhesion, and activation under physiologic flow. *J Exp Med*. 1998;188(8):1413–1419.
41. Goda S, et al. CX3C-chemokine, fractalkine-enhanced adhesion of THP-1 cells to endothelial cells through integrin-dependent and -independent mechanisms. *J Immunol*. 2000;164(8):4313–4320.
42. Wang CH, et al. Stem cell factor deficiency is vasculoprotective: unraveling a new therapeutic potential of imatinib mesylate. *Circ Res*. 2006;99(6):617–625.
43. Mombouli JV, Vanhoutte PM. Endothelial dysfunction: from physiology to therapy. *J Mol Cell Cardiol*. 1999;31(1):61–74.
44. Rubanyi GM. The role of endothelium in cardiovascular homeostasis and diseases. *J Cardiovasc Pharmacol*. 1993;22(suppl 4):S1–S14.
45. Chappell DC, Varner SE, Nerem RM, Medford RM, Alexander RW. Oscillatory shear stress stimulates adhesion molecule expression in cultured human endothelium. *Circ Res*. 1998;82(5):532–539.
46. Gimbrone MA Jr, Topper JN, Nagel T, Anderson KR, Garcia-Cardena G. Endothelial dysfunction, hemodynamic forces, and atherogenesis. *Ann N Y Acad Sci*. 2000;902:230–239; discussion 239–240.
47. Rao RM, Yang L, Garcia-Cardena G, Luscinskas FW. Endothelial-dependent mechanisms of leukocyte recruitment to the vascular wall. *Circ Res*. 2007;101(3):234–247.
48. Danenberg HD, et al. Systemic inflammation induced by lipopolysaccharide increases neointimal formation after balloon and stent injury in rabbits. *Circulation* 2002;105(24):2917–2922.
49. Shiba Y, et al. M-CSF accelerates neointimal formation in the early phase after vascular injury in mice: the critical role of the SDF-1-CXCR4 system. *Arterioscler Thromb Vasc Biol*. 2007;27(2):283–289.
50. Ikeda U, Shimada K. Matrix metalloproteinases and coronary artery diseases. *Clin Cardiol*. 2003; 26(2):55–59.
51. Cho A, Reidy MA. Matrix metalloproteinase-9 is necessary for the regulation of smooth muscle cell replication and migration after arterial injury. *Circ Res*. 2002;91(9):845–851.
52. Kuzuya M, et al. Deficiency of gelatinase a suppresses smooth muscle cell invasion and development of experimental intimal hyperplasia. *Circulation*. 2003;108(11):1375–1381.
53. Clowes AW, Reidy MA, Clowes MM. Kinetics of cellular proliferation after arterial injury. I. Smooth muscle growth in the absence of endothelium. *Lab Invest*. 1983;49(3):327–333.
54. Daginakatte GC, Gutmann DH. Neurofibromatosis-1 (Nf1) heterozygous brain microglia elaborate paracrine factors that promote Nf1-deficient astrocyte and glioma growth. *Hum Mol Genet*. 2007; 16(9):1098–1112.
55. Yang FC, et al. Nf1-dependent tumors require a microenvironment containing $Nf1^{+/-}$- and c-kit-dependent bone marrow. *Cell*. 2008;135(3):437–448.
56. Sironi M, et al. IL-1 stimulates IL-6 production in endothelial cells. *J Immunol*. 1989;142(2):549–553.
57. Iversen PO, Nicolaysen A, Kvernebo K, Benestad HB, Nicolaysen G. Human cytokines modulate arterial vascular tone via endothelial receptors. *Pflugers Arch*. 1999;439(1–2):93–100.
58. Bazan JF, et al. A new class of membrane-bound chemokine with a CX3C motif. *Nature*. 1997; 385(6617):640–644.
59. Imai T, et al. Identification and molecular characterization of fractalkine receptor CX3CR1, which mediates both leukocyte migration and adhesion. *Cell*. 1997;91(4):521–530.
60. Ancuta P, et al. Fractalkine preferentially mediates arrest and migration of CD16+ monocytes. *J Exp Med*. 2003;197(12):1701–1707.
61. Liu P, Patil S, Rojas M, Fong AM, Smyth SS, Patel DD. CX3CR1 deficiency confers protection from intimal hyperplasia after arterial injury. *Arterioscler Thromb Vasc Biol*. 2006;26(9):2056–2062.
62. Zhang YY, et al. *Nf1* regulates hematopoietic progenitor cell growth and ras signaling in response to multiple cytokines. *J Exp Med*. 1998;187(11):1893–1902.
63. Zhu Y, et al. Ablation of NF1 function in neurons induces abnormal development of cerebral cortex and reactive gliosis in the brain. *Genes Dev*. 2001; 15(7):859–876.
64. Okabe M, Ikawa M, Kominami K, Nakanishi T, Nishimune Y. 'Green mice' as a source of ubiquitous green cells. *FEBS Lett*. 1997;407(3):313–319.
65. Munugalavadla V, Borneo J, Ingram DA, Kapur R. p85alpha subunit of class IA PI-3 kinase is crucial for macrophage growth and migration. *Blood*. 2005;106(1):103–109.
66. [No authors listed]. Neurofibromatosis. Conference statement. National Institutes of Health Consensus Development Conference. *Arch Neurol*. 1988;45(5):575–578.
67. Yoder MC, et al. Redefining endothelial progenitor cells via clonal analysis and hematopoietic stem/progenitor cell principals. *Blood*. 2007; 109(5):1801–1809.